

光学学报

基于达曼光栅的快照式斯托克斯偏振测量方法

唐凡春^{1,2}, 步扬^{1,2*}, 吴芳³, 王向朝¹

¹中国科学院上海光学精密机械研究所信息光学与光电技术实验室, 上海 201800;

²中国科学院大学材料与光电研究中心, 北京 100049;

³张江实验室, 上海 201210

摘要 斯托克斯偏振测量常被用于获取光束的偏振特性。提出一种利用偏振无关的达曼光栅快照式测量偏振光束斯托克斯参量的方法。偏振光束通过达曼光栅后在空间对称的位置上被分成 4 束, 这 4 束光经波片和线偏振器调制后, 最终被 CCD 采集。将单次快照采集的光强图简单叠加运算就可计算得到偏振光束的斯托克斯参量, 并可进一步计算得到偏振光束的偏振分布、矢量质量因子(VQF)和模间相位。所提测量方法对不同椭圆偏振光的测量结果与商用偏振测量仪的测量结果之间的平均相对误差为 6.97%。所提方法的测量装置简单, 无需转动任何器件, 单次快照就可完成测量, 具有可靠的测量精度。

关键词 测量; 偏振测量; 斯托克斯参量; 达曼光栅

中图分类号 O436.3

文献标志码 A

DOI: 10.3788/AOS221731

1 引言

偏振是描述光波振动方向和振幅分布的一个重要参数, 在遥感技术、穆勒矩阵测量和生物学诊断等重要领域, 精确快速测量光束的偏振参数具有重要意义^[1-6]。光束的偏振特性常用斯托克斯参量来描述, 这是因为斯托克斯参量可以用来描述完全偏振光、部分偏振光和非偏振光^[7]。斯托克斯参量直接反映光束偏振分量的光强信息, 其所有参量都是实数值, 可以通过测量光强信息直接确定, 并且可用斯托克斯参量对光束的偏振分布和模间相位等参数进行重建^[8-9]。

斯托克斯参量的测量方法主要包括分时型、分光型等方法。分时型测量方法主要指在光路中通过旋转偏振光学元件来逐个测量需要的光强值, 或者按照特定的频率旋转偏振光学元件, 获得被调制的光强曲线, 最后利用测量结果计算得到待测光束的斯托克斯参量^[10-11]。分时型测量方法的主要缺点是测量耗时长且对待测光束稳定性的要求高, 旋转偏振光学元件会增加测量误差, 因此该测量方法无法测量偏振态实时变化的光束, 只能用于测量静态偏振目标光束。分光型测量方法可以克服分时型测量方法遇到的困难, 但也面临诸如装置复杂、光强分布不均和传播距离不同导致的光斑尺寸失配等问题^[12-13]。为实现对斯托克斯参量的实时测量, Gao 等^[14]使用涡旋半波片(VHW)对待

测光束进行空间调制, 并对单次采集的光强分布图进行拉东变换和傅里叶分析, 从而计算得到斯托克斯参量。但该方法无法测量待测光束斯托克斯参量的空间分布, 这意味着该方法无法测量偏振分布不均匀的矢量光束的斯托克斯参量。Zhao 等^[9]通过在数字微镜装置(DMD)上加载衍射光栅全息图, 将待测光束投影出 4 束相同的光束, 并对每束光分别进行不同的强度测量, 最后经透镜会聚后被 CCD 采集。该测量方法能够对矢量光束的斯托克斯参量进行实时测量, 并根据斯托克斯参量重建得到矢量光束的全场偏振分布。但 DMD 的衍射效率较低, 且投影的光束经过不同数量的光学元件后每束光的衰减程度相差较大, 这些都会影响斯托克斯参量的测量精度。

为克服上述测量方法存在的问题, 本文提出一种基于达曼光栅的斯托克斯参量测量方法。该测量方法通过达曼光栅将待测光束在空间上分成相同的 4 束, 经透镜准直后, 每束光沿空间对称的路径通过波片和线偏振器, 最后 4 束光同时被 CCD 采集。利用单次快照采集的光强图就能测量得到待测光束的斯托克斯参量。对不同模式的矢量光和圆偏振涡旋光的斯托克斯参量进行测量, 并根据测得的斯托克斯参量重建得到偏振分布, 实验结果与理论结果基本吻合。利用该测量方法测量不同椭圆偏振光的斯托克斯参量, 并将实验测量结果与商用偏振测量仪的测量结果进行对比,

收稿日期: 2022-09-22; 修回日期: 2022-11-08; 录用日期: 2023-03-03; 网络首发日期: 2023-03-13

基金项目: 国家科技重大专项(2016ZX02201-001)、上海市科委项目(18511104500)

通信作者: *buyang@siom.ac.cn

对比结果证明了所提测量方法的可行性和准确性。所提方法的测量装置简单,无需转动光学元件,测量速度快,操作方便。

2 原理

2.1 测量原理

达曼光栅是一种具有两个相位台阶的二元光学元件,具有尺寸小、衍射效率高、加工成本低等优点。通过控制两个台阶相位变换点的横向位置,达曼光栅可以得到激光远场多级谱点等强度的光点阵列^[15]。结合简化模式理论和严格耦合波分析进行矢量分析,可以设计出高效率、偏振无关的分束达曼光栅结构^[16]。该测量方法通过设计特定的达曼光栅结构实现。达曼光栅可以将入射光束进行分束,分成与其自身偏振特性相同的4束。这4束光在空间上沿光轴对称分布,形成一个光束的多重复制。

与均匀偏振光束不同,矢量光束的偏振自由度和空间自由度是不可分离的^[17]。矢量光可以在极坐标系中表示为左旋和右旋圆偏振涡旋光的叠加^[18],即

$$U(r, \phi) = \cos \alpha \exp(-il\phi e_R) + \sin \alpha \exp(il\phi) \exp(i\xi) e_L, \quad (1)$$

式中: r 为光场在坐标中的位置幅值; e_R 和 e_L 分别表示右旋圆偏振基矢和左旋圆偏振基矢; ξ 表示基矢的模间相位; $\exp(il\phi)$ 表示涡旋光的螺旋相位,其中 l 表示拓扑荷数, ϕ 表示方位角, i 为虚数单位; $\alpha \in [0, \pi/2]$ 为振幅因子。当 $\alpha=0$ 或 $\alpha=\pi/2$ 时, U 表示标量光场;当 $\alpha=\pi/4$ 时, U 表示矢量光场。

用来描述光束偏振态的斯托克斯参量是 4×1 的列向量,其4个参量具有不同的物理含义:第一个参量 S_0 描述光束的总光强值,第二个参量 S_1 描述光束的水平线偏振和垂直线偏振分量之差,第三个参量 S_2 描述光束的 $+45^\circ$ 线偏振和 -45° 线偏振分量之差,第四个参量 S_3 描述光束中包含的左旋圆偏振和右旋圆偏振分量之差^[7]。仅通过测量不同的光强值,即可从实验上测量得到斯托克斯参量,即

$$S = \begin{bmatrix} S_0 \\ S_1 \\ S_2 \\ S_3 \end{bmatrix} = \begin{bmatrix} I_0 \\ I_H - I_V \\ I_D - I_A \\ I_R - I_L \end{bmatrix}, \quad (2)$$

式中: I_0 表示光束的总光强; I_H 表示水平线偏振光强; I_V 表示垂直线偏振光强; I_D 表示 $+45^\circ$ 线偏振光强; I_A 表示 -45° 线偏振光强; I_R 表示右旋圆偏振光强; I_L 表示左旋圆偏振光强。由于 $I_0 = I_H + I_V = I_D + I_A = I_R + I_L$,只需要测量4个光强值即可确定光束的斯托克斯参量。

入射光束的斯托克斯参量为 $S = [S_0 \ S_1 \ S_2 \ S_3]^T$,被达曼光栅分束后分别通过4个不同的波片,得到

$$\left\{ \begin{array}{l} M_{HWP1}S = \begin{bmatrix} 1 & 0 & 0 & 0 \\ 0 & 1 & 0 & 0 \\ 0 & 0 & -1 & 0 \\ 0 & 0 & 0 & -1 \end{bmatrix} \begin{bmatrix} S_0 \\ S_1 \\ S_2 \\ S_3 \end{bmatrix} = \begin{bmatrix} S_0 \\ S_1 \\ -S_2 \\ -S_3 \end{bmatrix} \\ M_{HWP2}S = \begin{bmatrix} 1 & 0 & 0 & 0 \\ 0 & -1 & 0 & 0 \\ 0 & 0 & 1 & 0 \\ 0 & 0 & 0 & -1 \end{bmatrix} \begin{bmatrix} S_0 \\ S_1 \\ S_2 \\ S_3 \end{bmatrix} = \begin{bmatrix} S_0 \\ -S_1 \\ S_2 \\ -S_3 \end{bmatrix}, \\ M_{HWP3}S = \begin{bmatrix} 1 & 0 & 0 & 0 \\ 0 & 0 & 1 & 0 \\ 0 & 1 & 0 & 0 \\ 0 & 0 & 0 & -1 \end{bmatrix} \begin{bmatrix} S_0 \\ S_1 \\ S_2 \\ S_3 \end{bmatrix} = \begin{bmatrix} S_0 \\ S_2 \\ S_1 \\ -S_3 \end{bmatrix} \\ M_{QWP1}S = \begin{bmatrix} 1 & 0 & 0 & 0 \\ 0 & 0 & 0 & -1 \\ 0 & 0 & 1 & 0 \\ 0 & 1 & 0 & 0 \end{bmatrix} \begin{bmatrix} S_0 \\ S_1 \\ S_2 \\ S_3 \end{bmatrix} = \begin{bmatrix} S_0 \\ -S_3 \\ S_2 \\ S_1 \end{bmatrix} \end{array} \right., \quad (3)$$

式中: M_{HWP1} 、 M_{HWP2} 和 M_{HWP3} 均为半波片的穆勒矩阵,它们的快轴与 x 轴的夹角分别为 0° 、 45° 和 22.5° ; M_{QWP1} 为四分之一波片的穆勒矩阵,该波片的快轴与 x 轴的夹角为 45° 。光束最后通过透光轴沿水平方向的线偏振器后,得到

$$\left\{ \begin{array}{l} S_{out1} = M_P M_{HWP1}S = \frac{1}{2} \begin{bmatrix} S_0 + S_1 \\ S_0 + S_1 \\ 0 \\ 0 \end{bmatrix} \\ S_{out2} = M_P M_{HWP2}S = \frac{1}{2} \begin{bmatrix} S_0 - S_1 \\ S_0 - S_1 \\ 0 \\ 0 \end{bmatrix}, \\ S_{out3} = M_P M_{HWP3}S = \frac{1}{2} \begin{bmatrix} S_0 + S_2 \\ S_0 + S_2 \\ 0 \\ 0 \end{bmatrix}, \\ S_{out4} = M_P M_{QWP1}S = \frac{1}{2} \begin{bmatrix} S_0 - S_3 \\ S_0 - S_3 \\ 0 \\ 0 \end{bmatrix} \end{array} \right., \quad (4)$$

式中: S_{out1} 、 S_{out2} 、 S_{out3} 和 S_{out4} 分别为4束光通过波片和线偏振器后的斯托克斯参量; M_P 为透光轴沿水平方向的线偏振器的穆勒矩阵。4束光经缩束准直后被CCD单次同时采集,则4束光的光强值分别为

$$\left\{ \begin{array}{l} I_1 = \frac{1}{2}(S_0 + S_1) \\ I_2 = \frac{1}{2}(S_0 - S_1) \\ I_3 = \frac{1}{2}(S_0 + S_2) \\ I_4 = \frac{1}{2}(S_0 - S_3) \end{array} \right., \quad (5)$$

式中: I_1, I_2, I_3 和 I_4 分别为CCD采集的4束光的光强度。通过式(5)可得:

$$\begin{cases} S_0 = I_1 + I_2 \\ S_1 = I_1 - I_2 \\ S_2 = 2I_3 - (I_1 + I_2)^\circ \\ S_3 = I_1 + I_2 - 2I_4 \end{cases} \quad (6)$$

由式(6)可知,根据CCD单次快照采集的光强值就可以计算得到入射光束的斯托克斯参量。根据得到的斯托克斯参量,重建得到的入射光束的偏振分布^[19]为

$$\begin{cases} \psi = \frac{1}{2} \arctan\left(\frac{S_2}{S_1}\right) \\ \chi = \frac{1}{2} \arcsin\left(\frac{S_3}{S_0}\right) \end{cases} \quad (7)$$

式中: $\psi(0 \leq \psi \leq \pi), \chi\left(-\frac{\pi}{4} \leq \chi \leq \frac{\pi}{4}\right)$ 分别为光束中某点偏振椭圆的方位角和椭偏率。除了对入射光束的偏振分布进行重建,还可以计算得到光束的矢量质量因子(VQF) F_{VQ} 和模间相位 ζ ,即

$$F_{VQ} = \sqrt{1 - \frac{S_1^2}{S_0^2} - \frac{S_2^2}{S_0^2} - \frac{S_3^2}{S_0^2}} = |\sin(2\alpha)|, \quad (8)$$

$$\zeta(r, \phi) = \arctan\left[\frac{S_3(r, \phi)}{S_2(r, \phi)}\right], \quad (9)$$

式中: $S_i(i=0, 1, 2, 3)$ 为全局斯托克斯参量,可通过 $S = \int S(r_\perp) dr_\perp$ 求得,其中 $r_\perp = (x, y)$ 表示光场中某点位置。VQF可以用来表示光场的矢量特性,对于矢量光,如径向偏振光、角向偏振光及其他螺旋偏振光,它们的VQF为1,而线偏振、圆偏振等标量光场的VQF为0^[17, 20]。

2.2 待测光场产生

使用线偏振器、四分之一波片和VHW生成的椭圆偏振光束、偏振分布不均匀的矢量光束和圆偏振涡旋光束作为测量对象。为了方便描述矢量光束和圆偏振涡旋光束的产生原理,采用琼斯矢量和琼斯矩阵进行描述。VHW在通光孔径上对特定波长光束均产生90°的相位延迟,但它的快轴绕中心连续旋转,可用琼斯矩阵^[21]表示

$$T_m(\phi) = \begin{bmatrix} \cos(m\phi) & \sin(m\phi) \\ \sin(m\phi) & -\cos(m\phi) \end{bmatrix}, \quad (10)$$

式中: m 为VHW的级次。这里选用 $m=1$ 的VHW作为研究对象。不同方向的线偏振光经过VHW后会生成不同模式的矢量光。当入射光为水平线偏振或垂直线偏振的高斯光束时,其通过VHW后会分别生成径向偏振光或角向偏振光:

$$\begin{cases} \begin{bmatrix} \cos \phi & \sin \phi \\ \sin \phi & -\cos \phi \end{bmatrix} \begin{bmatrix} 1 \\ 0 \end{bmatrix} = \begin{bmatrix} \cos \phi \\ \sin \phi \end{bmatrix} \\ \begin{bmatrix} \cos \phi & \sin \phi \\ \sin \phi & -\cos \phi \end{bmatrix} \begin{bmatrix} 0 \\ 1 \end{bmatrix} = \begin{bmatrix} \sin \phi \\ -\cos \phi \end{bmatrix} \end{cases}. \quad (11)$$

圆偏振高斯光束通过VHW后会生成涡旋光,比如入射光为右旋圆偏振高斯光时,会生成携带拓扑荷数为1的左旋圆偏振涡旋光束:

$$\begin{bmatrix} \cos \phi & \sin \phi \\ \sin \phi & -\cos \phi \end{bmatrix} \begin{bmatrix} 1 \\ i \end{bmatrix} = \exp(i\phi) \begin{bmatrix} 1 \\ -i \end{bmatrix}. \quad (12)$$

3 实验与分析

3.1 实验装置

图1为实验装置示意图。实验中采用波长为632.8 nm的He-Ne激光器作为光源,其出射光的偏振态是随机的。线偏振器P1和P2为薄膜偏振片,其消光比大于5000:1。出射光经过P1和VHW后生成矢量光,改变P1的透光轴角度可以生成不同模式的矢量光。利用偏振无关的达曼光栅将矢量光在空间上分成相同的4束光,达曼光栅的栅距为10.128 μm×10.128 μm。这4束光经过焦距为200 mm的平凸透镜L1后都变成准直光束。4束准直光束分别通过半波片HWP1、HWP2、HWP3和四分之一波片QWP1,3个半波片的快轴与x轴的夹角分别为0°、45°和22.5°,四分之一波片的快轴与x轴的夹角为45°,它们都为聚合物零级波片,相位延迟量精度为3.6°($\lambda/100$, λ 为He-Ne激光器的出射光波长632.8 nm)。WH为所设计的波片载具,其4个通光孔用于安装波片,不透光的部分用来滤去包括零级衍射级次的多余衍射光束。L2和L3分别为200 mm焦距的平凸透镜和75 mm焦距的平凹透镜,它们组成一个缩束系统,用于将4束光缩束到合适的尺寸并进行准直。最后,4束光经过透光轴沿水平方向的P2和中性密度滤光片NDF后被CCD记录。CCD的像素为1936 pixel×1216 pixel,单个像素的尺寸为5.86 μm×5.86 μm。

3.2 矢量光束和圆偏振涡旋光束的斯托克斯参量测量

将P1的透光轴置于水平方向,VHW的零度快轴置于水平方向,此时激光器出射光通过P1和VHW后生成径向偏振光。在未插入WH和P2的情况下对光路进行对准,径向偏振光经达曼光栅分成4束后最终被CCD采集,采集的光强如图2所示。图2中每个光斑的直径约占180个像素点,即光斑直径约为1.05 mm,而中心光斑为达曼光栅的零级衍射级次光斑。对图2中外围的4个光斑进行相似度分析,相似度为99.3%,可知入射到达曼光栅的径向偏振光被很好地分成了4束。利用图2采集的光斑对光斑中心位置

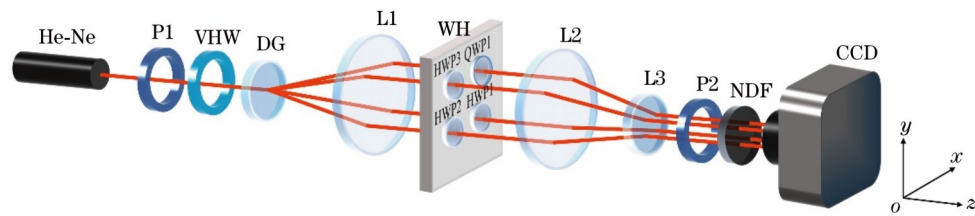


图1 实验装置示意图
Fig. 1 Schematic of experimental setup

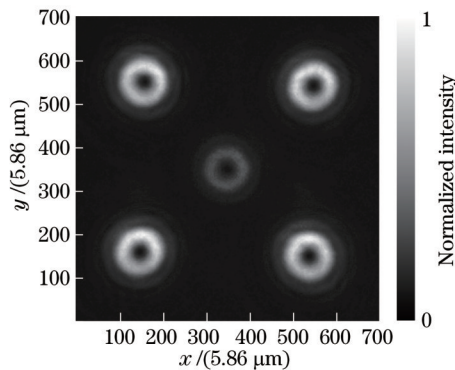


图2 CCD采集的经达曼光栅分束的径向偏振光
Fig. 2 Radially polarized beam divided Dammann grating and captured by CCD

进行定标,从而方便后续对光斑进行处理。

对实验装置进行对准后,在光路中插入WH和P2,并在WH的4个通光孔中分别安装半波片HWP1、HWP2、HWP3和四分之一波片QWP1,3个半波片的快轴与x轴的夹角分别为 0° 、 45° 和 22.5° ,四分之一波片的快轴与x轴的夹角为 45° ,它们的安装位置如图1所示。CCD采集的光强如图3所示。根据图3的实验测量结果,利用式(6)可计算得到径向偏振光的斯托克斯参量,实验测量结果如图4所示。图3和图4都给出了对应的理论仿真结果,可以看到,实验测量结果和理论仿真结果吻合得较好。根据计算得到的斯托克斯参量可重建径向偏振光的偏振分布,由图5可知,实验测量结果和仿真计算结果基本一致。

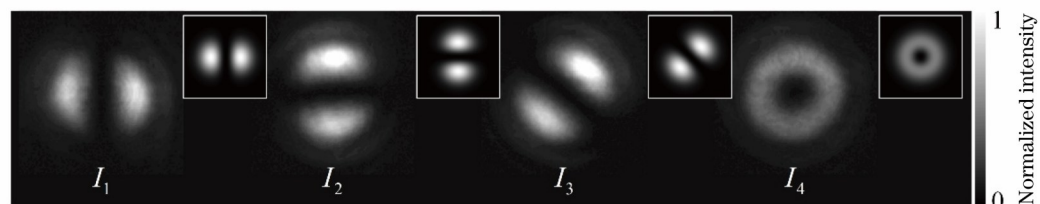


图3 径向偏振光的实验测量结果,插图为理论仿真结果
Fig. 3 Experimental measurement results of radially polarized beam, and the inserts are theoretical simulation results

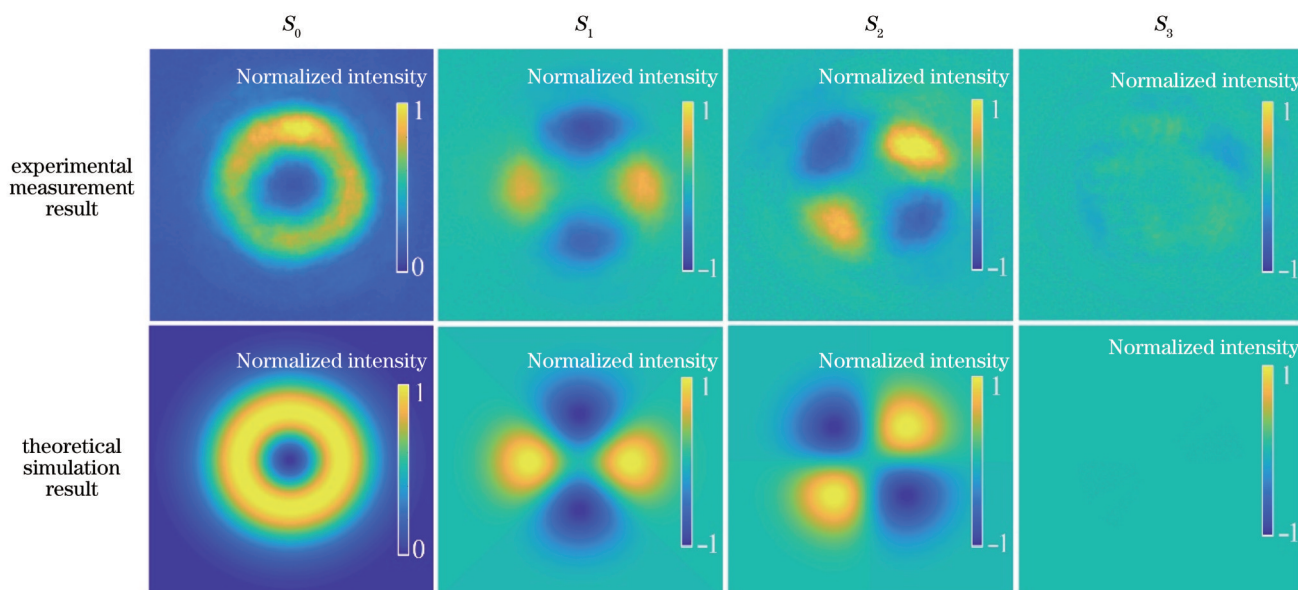


图4 径向偏振光的斯托克斯参量
Fig. 4 Stokes parameters of radially polarized beam

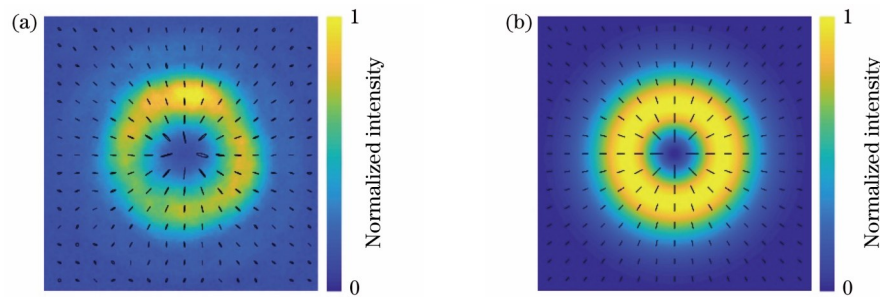


图5 径向偏振光的重建偏振分布。(a)实验测量结果;(b)理论仿真结果

Fig. 5 Reconstructed polarization distribution of radially polarized beam. (a) Experimental measurement result; (b) theoretical simulation result

在实验中,旋转P1可以改变经过VHW后出射光的偏振态。旋转P1,取其透光轴与水平方向的夹角 θ_1 为30°、60°和90°时,可以得到其他模式的矢量光束。当 θ_1 为90°时,激光器的出射光经过P1和VHW后会生成角向偏振光。图6(a)~(c)给出了根据实验测量的斯托克斯参量重建的不同偏振光束的偏振分布结果。

除了矢量偏振光束外,该测量方法还可对标量偏振光束的斯托克斯参量进行测量。在P1和VHW中间插入四分之一波片QWP2,并使其快轴与水平方向的夹角 θ_2 为45°,这时激光器出射光经过P1和

QWP2后生成右旋圆偏振光。由式(12)可知,右旋圆偏振光照射VHW后会生成左旋圆偏振涡旋光。对左旋圆偏振涡旋光的斯托克斯参量进行测量并重建其偏振分布,实验测量结果如图6(d)所示,其中黑色表示左旋偏振,白色表示右旋偏振。图6同样给出了对应的理论仿真结果,对比可知,实验测量结果与理论仿真结果吻合得较好。图5和图6所示的偏振分布图中都存在部分边缘没有偏振椭圆的情形,这是因为在重建待测偏振光束的偏振分布过程中,图像中某些位置归一化的 S_0 太小,导致该位置的偏振椭圆无法显示。

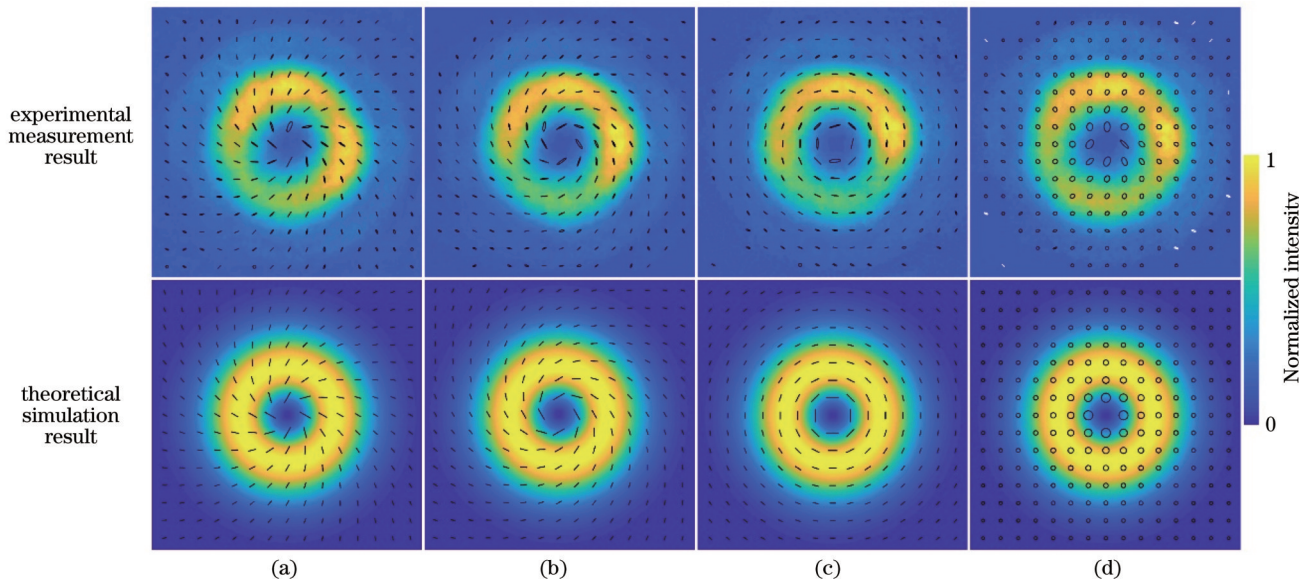


图6 基于不同偏振光束重建的偏振分布。(a) $\theta_1=30^\circ$; (b) $\theta_1=60^\circ$; (c) $\theta_1=90^\circ$; (d) $\theta_1=0^\circ, \theta_2=45^\circ$

Fig. 6 Reconstructed polarization distribution based on different polarized beams. (a) $\theta_1=30^\circ$; (b) $\theta_1=60^\circ$; (c) $\theta_1=90^\circ$; (d) $\theta_1=0^\circ, \theta_2=45^\circ$

3.3 椭圆偏振光的斯托克斯参量测量

目前大多数商用偏振测量仪只能测量均匀偏振光束的偏振态,无法测量矢量光的空间偏振分布,导致所提测量方法在测量矢量光的斯托克斯参量时,无法将实验测量结果与其他仪器的测量结果进行定量比较分析。为了进一步验证所提测量方法的可行性和准确度,利用P1和消色差四分之一波片(AQWP)生成不同

的椭圆偏振光,将所提测量方法对椭圆偏振光的实验测量结果与Thorlabs的商用偏振测量仪的测量结果进行对比。He-Ne激光器出射激光通过P1和AQWP后生成椭圆偏振光,旋转AQWP可以改变椭圆偏振光的偏振态。AQWP在632.8 nm处的相位延迟量为87.04°,相位延迟量精度为1.2°($\lambda/300$)。使用的商用偏振测量仪可以测量均匀偏振光束的斯托克斯参量,

其偏振度测量精度为1%。

将图1所示实验装置中的VHW换成AQWP,使P1的透光轴沿水平方向,AQWP的初始快轴沿水平方向,将AQWP每次旋转20°,对AQWP在不同快轴角度下生成的椭圆偏振光进行斯托克斯参量测量。该测量方法可以测量椭圆偏振光的全场斯托克斯参量,取中心固定区域的平均值作为实验测量值。利用商用偏振测量仪测量不同椭圆偏振光的斯托克斯参量。表1给出了所提测量方法和商用偏振测量仪分别测得的不同椭圆偏振态的归一化斯托克斯参量。图7所示的庞

加莱球给出了不同椭圆偏振态的理论斯托克斯参量值和两种测量方法的测量值。将所提测量方法的测量值与商用偏振测量仪的测量值进行比较,记庞加莱球上两种测量方法的测量值表示点之间的距离为相对误差^[22],表1给出了不同椭圆偏振态下两种测量方法测量值之间的相对误差。针对不同偏振态的椭圆偏振光,所提测量方法和商用偏振测量仪的测量结果之间的平均相对误差为6.97%,表明所提测量方法具有可行性和准确性。

表1 18个椭圆偏振态的偏振测量仪的测量值和实验测量值

Table 1 Measured value obtained by polarimeter and experimental value of 18 elliptical polarization states

| Elliptical polarization | Polarimetry value of $[S_1, S_2, S_3]$ | Experimental value of $[S_1, S_2, S_3]$ | Relative error /% |
|-------------------------|--|---|-------------------|
| Case 1 | [0.64, 0.43, 0.63] | [0.62, 0.46, 0.56] | 7.87 |
| Case 2 | [0.18, 0.14, 0.97] | [0.10, 0.06, 0.93] | 12.00 |
| Case 3 | [0.37, -0.36, 0.85] | [0.39, -0.37, 0.81] | 4.58 |
| Case 4 | [0.89, -0.29, 0.35] | [0.83, -0.31, 0.45] | 11.83 |
| Case 5 | [0.90, 0.29, -0.33] | [0.81, 0.26, -0.35] | 9.70 |
| Case 6 | [0.28, 0.41, -0.86] | [0.29, 0.34, -0.86] | 7.07 |
| Case 7 | [0.03, -0.17, -0.98] | [0.05, -0.18, -1.00] | 3.00 |
| Case 8 | [0.57, -0.52, -0.63] | [0.57, -0.48, -0.66] | 5.00 |
| Case 9 | [1.00, -0.01, -0.01] | [0.95, -0.03, -0.03] | 5.74 |
| Case 10 | [0.50, 0.54, 0.63] | [0.51, 0.51, 0.65] | 3.74 |
| Case 11 | [-0.06, 0.21, 0.98] | [-0.01, 0.13, 0.92] | 11.18 |
| Case 12 | [0.18, -0.48, 0.86] | [0.27, -0.45, 0.84] | 9.70 |
| Case 13 | [0.87, -0.34, 0.34] | [0.82, -0.34, 0.38] | 6.40 |
| Case 14 | [0.88, 0.33, -0.33] | [0.86, 0.37, -0.33] | 4.47 |
| Case 15 | [0.26, 0.44, -0.86] | [0.26, 0.43, -0.86] | 1.00 |
| Case 16 | [0.07, -0.16, -0.98] | [0.05, -0.13, -0.95] | 4.69 |
| Case 17 | [0.63, -0.45, -0.63] | [0.56, -0.43, -0.58] | 8.83 |
| Case 18 | [1.00, 0.01, 0.01] | [0.96, 0.04, 0.08] | 8.60 |

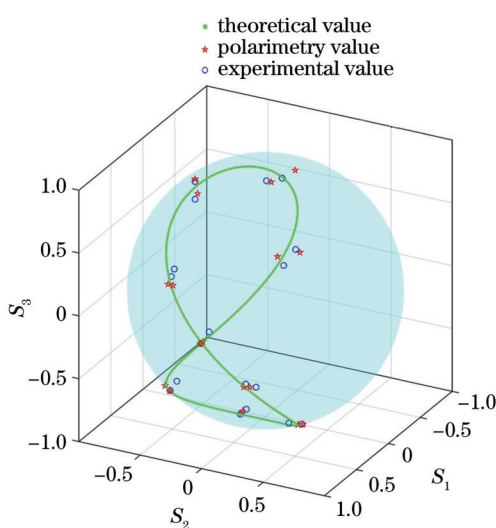


图7 庞加莱球上椭圆偏振光的斯托克斯参量

Fig. 7 Stokes parameters of elliptically polarized beams on a Poincaré sphere

3.4 VQF和模间相位的测量结果

根据测得的斯托克斯参量,利用式(8)和式(9)可以计算得到偏振光束的VQF和模间相位,表2给出了矢量光束和圆偏振涡旋光束的实验测量结果和理论仿真结果。从表2可见,待测光束的VQF的实验测量值与理论仿真值非常接近,尤其是矢量偏振光,而模间相位的实验测量结果和理论仿真结果也能很好地匹配。VQF可以定量地描述偏振光束的模式纯度,其实验结果从侧面验证了该测量方法的有效性。

4 误差分析

实验系统中,波片的相位延迟量偏差 $\Delta\delta$ 、波片的快轴方位角偏差 $\Delta\beta$ 和线偏振器的透光轴角度偏差 $\Delta\theta$ 是入射光束斯托克斯参量测量精度的主要影响因素。以径向偏振光为分析对象,考虑到实验中使用的波片的相位延迟量精度为3.6°($\lambda/100$),波片的快轴方位角和线偏振器的透光轴角度偏差主要由本身的制作误差和安装座的旋转精度决定,实验中安装座的旋转精度

表2 不同偏振光束的VQF和模间相位

Table 2 VQF and intra-modal phase of different polarized beams

| Polarized beam | $\theta_1 = 0^\circ$ | $\theta_1 = 30^\circ$ | $\theta_1 = 60^\circ$ | $\theta_1 = 90^\circ$ | $\theta_1 = 0^\circ$, $\theta_2 = 45^\circ$ | |
|----------------------|----------------------|-----------------------|-----------------------|-----------------------|---|--|
| VQF | Experimental result | 0.9972 | 0.9962 | 0.9957 | 0.9972 | |
| | Theoretical result | 1 | 1 | 1 | 0 | |
| Intra-modal phase | Experimental result | | | | | |
| | Theoretical result | | | | | |

为 1° , 分别对波片相位延迟量偏差 $\Delta\delta = 3.6^\circ$ 、波片的快轴方位角偏差 $\Delta\beta = 1^\circ$ 和线偏振器透光轴角度偏差 $\Delta\theta = 1^\circ$ 的情况进行误差分析。

图8所示为波片相位延迟量存在 3.6° 偏差时径向偏振光斯托克斯参量测量误差的仿真结果, 图9和图10所示分别为波片快轴方位角存在 1° 偏差和线偏振器透光轴角度存在 1° 偏差时斯托克斯参量测量误差的仿真结果。从图8~10可以分析出, 斯托克斯参

量的测量误差与入射光束的光强分布和偏振分布有关, 即这些偏差因素对具有不同光强分布和偏振态的光束的斯托克斯参量测量影响不同。波片的相位延迟量偏差对斯托克斯不同参量的测量结果影响不同, 其中对 S_3 测量结果的影响相对于 S_1 和 S_2 较大。波片快轴方位角偏差和线偏振器透光轴角度偏差对斯托克斯参量测量误差的影响相当。 $\Delta\delta$ 、 $\Delta\beta$ 和 $\Delta\theta$ 带来的最大综合误差约为0.09, 即9%。

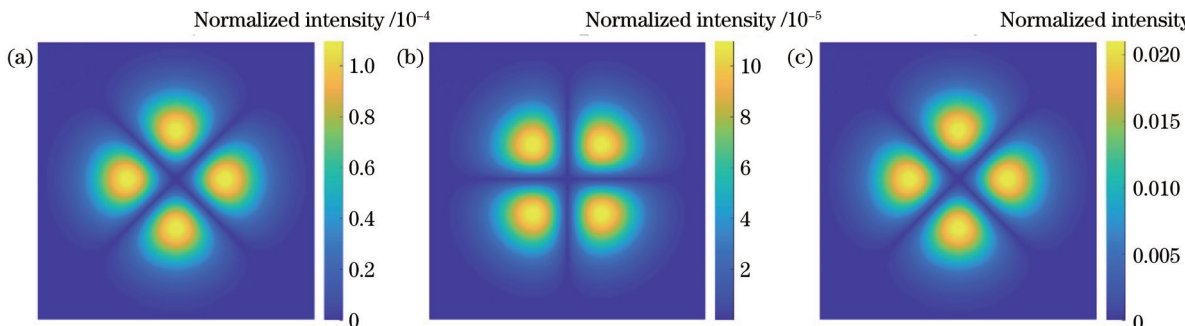
图8 波片相位延迟量存在 3.6° 偏差时径向偏振光的斯托克斯参量测量误差。(a) ΔS_1 ; (b) ΔS_2 ; (c) ΔS_3

Fig. 8 Stokes parameter measurement errors of radially polarized beams when the phase retardation of the wave plate has a deviation of 3.6° . (a) ΔS_1 ; (b) ΔS_2 ; (c) ΔS_3

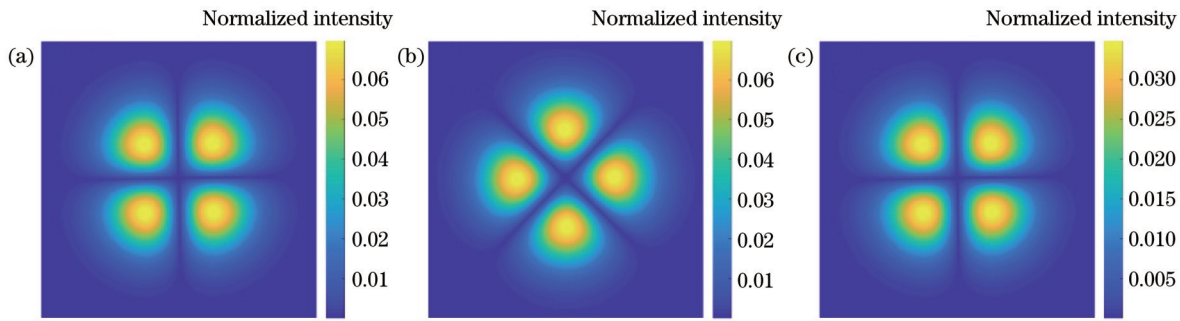
图9 波片快轴方位角存在 1° 偏差时径向偏振光的斯托克斯参量测量误差。(a) ΔS_1 ; (b) ΔS_2 ; (c) ΔS_3

Fig. 9 Stokes parameter measurement errors of radially polarized beams when the fast axis azimuth of the wave plate has a deviation of 1° . (a) ΔS_1 ; (b) ΔS_2 ; (c) ΔS_3

表1中, 所提测量方法和商用偏振测量仪针对不同椭圆偏振光的最大相对测量误差为12%。考虑到CCD噪声、线偏振器消光比和人为操作等因素带来的

影响, 12%的相对测量误差与误差分析得到的最大综合误差相当。

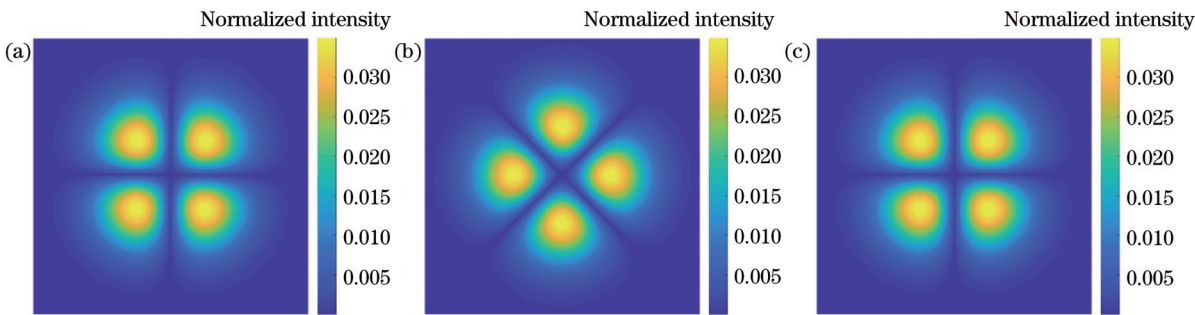


图10 偏振器透光轴角度存在 1° 偏差时径向偏振光的斯托克斯参量测量误差。(a) ΔS_1 ; (b) ΔS_2 ; (c) ΔS_3

Fig. 10 Stokes parameter measurement errors of radially polarized beams when the polarization transmittance axis angle of the polarizer has a deviation of 1° . (a) ΔS_1 ; (b) ΔS_2 ; (c) ΔS_3

5 结 论

基于达曼光栅的分束功能,提出一种单次快照式测量任意偏振光束斯托克斯参量的方法。该测量方法利用达曼光栅将待测光束生成相同的4束光,经透镜准直后,4束光分别经过不同的波片,被缩束后经过线偏振器并最终被CCD采集。根据CCD单次采集的强度分布图,通过简单计算就可得到待测光束的斯托克斯参量。实验中对多种矢量光和圆偏振涡旋光的斯托克斯参量进行测量,根据测得的斯托克斯参量重建得到待测光束的偏振分布、VQF和模间相位。实验测量结果和理论仿真结果吻合得较好。利用所提测量方法对多种椭圆偏振光的斯托克斯参量进行测量,该方法的测量结果与商用偏振测量仪测量结果之间的平均相对误差为6.97%,从而验证了该测量方法的可行性和准确性。所提方法所使用的达曼光栅是根据待测光束波长和需要的分离角设计的,达曼光栅能够接受较宽范围的入射光束的光斑直径,且该达曼光栅对入射光束的偏振没有要求,所以该测量装置具有一定的通用性。所提出的斯托克斯偏振测量方法简单,测量结果可靠,且不需要使用全数字控制的器件,有效降低了成本。后续使用相位延迟量精度更高的波片和旋转精度更高的安装台可进一步提高测量精度。

参 考 文 献

- [1] Yan L, Li Y F, Chandrasekar V, et al. General review of optical polarization remote sensing[J]. International Journal of Remote Sensing, 2020, 41(13): 4853-4864.
- [2] Tu H T, Zheng Y X, Shan Y, et al. High-performance ellipsometry with 2-D expanded channels for spectroscopy and polarization analysis[J]. IEEE Transactions on Instrumentation and Measurement, 2021, 70: 7006308.
- [3] Ushenko V O, Trifonyuk L, Ushenko Y A, et al. Polarization singularity analysis of Mueller-matrix invariants of optical anisotropy of biological tissues samples in cancer diagnostics[J]. Journal of Optics, 2021, 23(6): 064004.
- [4] 王文爱, 马紫瑜, 李佳蓓, 等. 穆勒成像偏振仪在病理诊断中的可靠性研究[J]. 光学学报, 2022, 42(15): 1512002.
Wang W A, Ma Z Y, Li J B, et al. Reliability of Mueller imaging polarimeter in pathological diagnosis[J]. Acta Optica Sinica, 2022, 42(15): 1512002.
- [5] de Sande J C G, Piquero G, Santarsiero M. Polarimetry with azimuthally polarized light[J]. Optics Communications, 2018, 410: 961-965.
- [6] 罗海波, 曹军峰, 盖兴琴, 等. 基于偏振成像的工业视觉及其关键技术[J]. 激光与光电子学进展, 2022, 59(14): 1415003.
Luo H B, Cao J F, Gai X Q, et al. Industrial vision based on polarization imaging and its key technologies[J]. Laser & Optoelectronics Progress, 2022, 59(14): 1415003.
- [7] Goldstein D H. Polarized light[M]. 3th ed. Florida: CRC Press, 2017.
- [8] Manthalkar A, Nape I, Bordbar N T, et al. All-digital Stokes polarimetry with a digital micromirror device[J]. Optics Letters, 2020, 45(8): 2319-2322.
- [9] Zhao B, Hu X B, Rodríguez-Fajardo V, et al. Real-time Stokes polarimetry using a digital micromirror device[J]. Optics Express, 2019, 27(21): 31087-31093.
- [10] Giudicotti L, Brombin M. Data analysis for a rotating quarter-wave, far-infrared Stokes polarimeter[J]. Applied Optics, 2007, 46(14): 2638-2648.
- [11] Schaefer B, Collett E, Smyth R, et al. Measuring the Stokes polarization parameters[J]. American Journal of Physics, 2007, 75(2): 163-168.
- [12] Azzam R M A. Division-of-amplitude photopolarimeter (DOAP) for the simultaneous measurement of all four Stokes parameters of light[J]. Optica Acta: International Journal of Optics, 1982, 29(5): 685-689.
- [13] Fridman M, Nixon M, Grinvald E, et al. Real-time measurement of space-variant polarizations[J]. Optics Express, 2010, 18(10): 10805-10812.
- [14] Gao C, Lei B. Spatially modulated polarimetry based on a vortex retarder and Fourier analysis[J]. Chinese Optics Letters, 2021, 19(2): 021201.
- [15] Dammann H, Görtler K. High-efficiency in-line multiple imaging by means of multiple phase holograms[J]. Optics Communications, 1971, 3(5): 312-315.
- [16] 周常河. 达曼光栅原理及应用[M]. 北京: 科学出版社, 2017.
Zhou C H. Principle and application of Dammann grating[M]. Beijing: Science Press, 2017.
- [17] Selyem A, Rosales-Guzmán C, Croke S, et al. Basis-independent tomography and nonseparability witnesses of pure complex vectorial light fields by Stokes projections[J]. Physical Review A, 2019, 100(6): 063842.
- [18] Galvez E J, Rojec B L, Kumar V, et al. Generation of isolated asymmetric umbilics in light's polarization[J]. Physical Review A, 2014, 89(3): 031801.
- [19] Singh K, Tabebordbar N, Forbes A, et al. Digital Stokes polarimetry and its application to structured light: tutorial[J]. Journal of the Optical Society of America A, 2020, 37(11): C33-C44.
- [20] Ndagano B, Sroor H, McLaren M, et al. Beam quality measure

- for vector beams[J]. Optics Letters, 2016, 41(15): 3407-3410.
- [21] 孙汝生, 刘通, 王琛, 等. 基于级联涡旋半波片的高阶柱矢量光束产生及其偏振检测[J]. 光学学报, 2022, 42(13): 1326001.
Sun R S, Liu T, Wang C, et al. High-order cylindrical vector beam generation and its polarization detection based on cascade vortex half-wave plates[J]. Acta Optica Sinica, 2022, 42(13): 1326001.
- [22] Yang Z Y, Wang Z K, Wang Y X, et al. Generalized Hartmann-Shack array of dielectric metalens sub-arrays for polarimetric beam profiling[J]. Nature Communications, 2018, 9(1): 1-7.

Snapshot Stokes Polarimetry Method Based on Dammann Grating

Tang Fanchun^{1,2}, Bu Yang^{1,2*}, Wu Fang³, Wang Xiangzhao¹

¹Laboratory of Information Optics and Opto-Electronic Technology, Shanghai Institute of Optics and Fine Mechanics, Chinese Academy of Sciences, Shanghai 201800, China;

²Center of Materials Science and Optoelectronics Engineering, University of Chinese Academy of Sciences, Beijing 100049, China;

³Zhangjiang Laboratory, Shanghai 201210, China

Abstract

Objective Polarization is a key parameter of light, accurate and rapid measurement of which plays a significant role in a variety of areas such as remote sensing technology, Mueller matrix measurement, and biological diagnosis. Stokes parameters directly reflect the light intensity of the polarization component of light, and all parameters can be directly determined by the measurement of light intensity. On this basis, the polarization distribution, vector quality factor, and intra-modal phase can be measured. The measurement methods of Stokes parameters mainly include the division-of-time and division-of-amplitude methods. The division-of-time method refers to the measurement of required intensities one by one, which is only applicable to static polarized light. The division-of-amplitude method can overcome shortcomings encountered by the division-of-time method, but it also faces many problems such as the complexity of the device, the uneven distribution of light intensity, and different propagation distances. In this study, a Stokes polarimetry method based on a polarization-insensitive Dammann grating is proposed. The Stokes parameters of the polarized beam can be calculated by the intensity spots in a single snapshot, and the polarization distribution, vector quality factor, and intra-modal phase of the polarized beam can be further obtained. This method has simple measuring equipment and does not need any rotating components. The measurement can be completed with a snapshot and has reliable accuracy.

Methods The measurement principle of the proposed method is described in Fig. 1. Formulas for calculating Stokes parameters, the polarization distribution, the vector quality factor, and the intra-modal phase of the polarized light are derived. The experimental setup is built upon the measurement principle. In the experiment, different vector polarized beams, circularly polarized beams, and elliptically polarized beams are generated to measure the target polarized beam. The polarization-insensitive Dammann grating is used to divide the incident polarized beam into four identical beams in a spatially symmetrical position. After being collimated by a convex lens, four beams are modulated by wave plates and a polarizer and finally captured by a CCD. Via the captured intensity images, Stokes parameters of the measured polarized beam are calculated, and the polarization distribution, vector quality factor, and the intra-modal phase of the polarized light beam are obtained. Finally, according to the measurement principle, we analyze the influence of the phase retardation deviation and fast axis azimuth deviation of wave plates and the transmittance axis deviation of the polarizer on Stokes parameter measurement.

Results and Discussions First, the generated radially polarized beam is used for the initial calibration, which is divided into four identical beams, as shown in Fig. 2. Four light spots recorded in Fig. 2 are used to calibrate the center position of the light spot, which is beneficial to the subsequent measurement. After that, the radially polarized beam is measured. On the basis of the four light spots recorded in a snapshot (Fig. 3), Stokes parameters of the radially polarized beam are calculated (Fig. 4), and then the polarization distribution is reconstructed (Fig. 5). The above experimental measurement results are all compared to the corresponding theoretical simulation results, and they have a good agreement. Then, more polarized beams are measured, and their experimental measurement results of reconstructed polarization distribution conform well to the theoretical simulation results (Fig. 6). The measurement results of the generated elliptically polarized beams are compared with those of the commercial polarimeter to verify the feasibility and accuracy of the measurement method. Table 1 shows the relative measurement errors of different elliptically polarized beams between the proposed

measurement method and the polarimeter, and the average relative error is 6.97%, which indicates the feasibility and accuracy of the proposed method. Additionally, the vector quality factor and intra-modal phase of different polarized beams are measured. At last, the analysis of the influence of some existing errors on Stokes parameter measurement shows that the phase retardation deviation and fast axis azimuth deviation of wave plates and the transmittance axis deviation of the polarizer could bring about a maximum measurement error of around 9% to Stokes parameter measurement.

Conclusions This study proposes a method of measuring Stokes parameters of arbitrary polarized beams based on a polarization-insensitive Dammann grating with a snapshot. The Dammann grating is used to divide the incident polarized beam into four identical beams in a spatially symmetrical position. After being collimated by the lens, the four beams pass through different wave plates and a polarizer and are eventually captured by a CCD. The Stokes parameters of the polarized beam can be calculated by a simple superposition of the intensity spots in a single snapshot, and the polarization distribution, vector quality factor, and intra-modal phase of the polarized beam can be further obtained. The experimental measurement results are in good agreement with the theoretical simulation results. The average relative error of elliptically polarized beams between the proposed measurement method and the commercial polarimeter is 6.97%, which verifies the feasibility and accuracy of this measurement method. The Dammann grating used in this method is designed according to the wavelength of the incident beam and the required separation angle. It can accept the spot diameter of the incident beam in a wide range and has no requirements for the polarization of the incident beam. Hence, the measuring device has certain universality. The proposed Stokes polarimetry method is simple and can obtain reliable results without all-digital devices, which effectively reduces the cost. The subsequent use of wave plates with higher precision of phase retardation and rotation mounts with higher precision of rotation can further improve the measurement accuracy.

Key words measurement; polarimetry; Stokes parameter; Dammann grating